Domain dynamics in the anisotropic Swift-Hohenberg equation

Katsuya Ouchi*
Kobe Design University, 8-1-1 Gakuennishi-Machi, Nishi-ku, Kobe 651-2196, Japan

Hirokazu Fujisaka†
Department of Applied Analysis and Complex Dynamical Systems, Graduate School of Informatics, Kyoto University, Kyoto 606-8501, Japan

(Received 23 March 2004; published 27 September 2004)

Two types of asymptotic ordering processes in the anisotropic Swift-Hohenberg equation are studied, paying particular attention to the interaction between domain walls. For the first type, we will discuss the time evolution in which the spatially oscillatory patterns are formed, and show that two kinds of patterns exist depending on whether or not the imaginary part of the field vanishes. When the imaginary part is present, the equation has two distinct states which are regarded as kinds of domains, so the dynamics between two domain walls is established. We then discuss, for the second type, the dynamics when nontrivial uniform states are constructed. There exist two different domain walls, the Néel type wall and the Bloch type wall, in a similar way to the anisotropic Ginzburg-Landau equation. The equation of motion for two domain walls is derived, and it is shown that the distance between the two domain walls eventually approaches a finite length. The theoretical result is confirmed by numerical simulations. This fact proves the validity of the prediction on the temporal development of the distance between two domain walls.

DOI: 10.1103/PhysRevE.70.036210 PACS number(s): 89.75.Kd, 75.10.−b, 75.30.Gw, 75.60.Ch

I. INTRODUCTION

There are many works on ordering processes associated with thermodynamic phase transitions [1–3] in magnetic systems and binary alloys. On the other hand, pattern formation processes in systems far from equilibrium, e.g., the Rayleigh-Bénard convection for liquid layers heated from below [4,5], liquid crystals under an oscillating electric field [6,7], chemical reaction-diffusion systems [8], etc., have been extensively studied from the theoretical as well as experimental points of view. A common approach to study the dynamics of domain walls associated with the ordering processes has been developed, and is now one of the prevailing methods to comprehensively understand such processes [9–14] despite the mechanisms of the above two kinds of processes being different from each other in the sense that the former evolves in time towards thermal equilibrium while the latter describes nonequilibrium and open systems. This fact shows a universal aspect of the ordering processes.

The present work was motivated by several recent experiments investigating the formation processes of magnetic domain structures and their statistical characteristics in garnet thin film under a temporally periodic external field [15,16]. It has been observed that the garnet thin film, which is one of the materials to form a ferromagnetic phase, constructs several spatial patterns, e.g., labyrinth, lamellar, triangular lattice, and spotty patterns, etc., depending on values of amplitude and frequency of the external magnetic field. The existence of the formation of lamellar patterns suggests that the system is capable of being phenomenologically represented in terms of the Swift-Hohenberg (SH) equation, the well-known model of the Rayleigh-Bénard convection [17]. The model turns out to be quite suitable to describe the formation process of the spatially oscillatory dissipative structures in systems far from equilibrium even though the ordering process in the garnet thin film is associated with thermodynamic phase transition. In fact, a labyrinth pattern is observed in the ferromagnetic system without applying an external field [16] where the temperature is kept far below the Curie temperature. The observed pattern is similar to that found in the SH equation when the control parameter corresponding to the temperature difference from the Curie temperature is sufficiently large [18,19].

Thus the simplest model to explain the experiment noted above may be the SH equation with an external field

$$\dot{w} = [\epsilon - (\nabla^2 + k_0^2)^2]w - w^3 + F(t), \tag{1}$$

where w is a real field corresponding to local magnetization, ϵ is a control parameter and k_0 is the wave number to be determined by the characteristics of the system as well as the boundary condition. In spite of k_0 being set to be unity by a simple rescaling, we will use k_0 in this paper because we adopted several values different from unity in numerical simulations. $F(t)$ is an external field, which is often represented as the sinusoidal force $F(t)=A\cos(\Omega t)$ with amplitude A and frequency Ω. However, it is known that the thin garnet film is a strongly anisotropic material. This fact suggests the necessity of extending the field w to a complex variable and then adding an anisotropic term γw^* to the complex SH equation as follows:

*Electronic address: ouchi@kobe-du.ac.jp
†Electronic address: fujisaka@i.kyoto-u.ac.jp

$$\dot{w} = [\epsilon - (\nabla^2 + k_0^2)^2]w - |w|^2 w + \gamma w^* + F(t) = -\frac{\delta \mathcal{H}}{\delta w^*}, \tag{2}$$

where w is a complex field and γ is the strength of the anisotropy, which is assumed to be real. $\mathcal{H}$ is the Lyapunov functional defined by

$$\mathcal{H} = \int d\mathbf{r}\Bigg[-\epsilon|w|^2 - \frac{\gamma}{2}(w^2 + w^{*2}) + \frac{1}{2}(|w|^2)^2 + |(\nabla^2 + k_0^2)w|^2 - F(t)(w + w^*)\Bigg]. \tag{3}$$

Equation (2) is hereafter referred to as the anisotropic Swift-Hohenberg (aSH) equation.

In this paper, we focus our discussion on the spatially one-dimensional (1D) system to reveal the fundamental characteristics of Eq. (2) in the absence of an external field, i.e., $F(t)=0$. We will show that the system exhibits several patterns depending on the control parameters ϵ and γ. The temporal evolution of the system will then be discussed in terms of the dynamics for the domain wall.

The present paper is constructed as follows. In Sec. II two types of oscillatory patterns, separated by the existence or absence of the imaginary part of the field, are discussed. The domain wall dynamics of the pattern with an imaginary part is further discussed in a similar way as for the time-dependent Ginzburg-Landau (TDGL) equation. It will be shown that the distance between neighboring walls develops logarithmically in time. In Sec. III it is found that a pair of nontrivial uniform states ($|w| \neq 0$) stably exists for a definite parameter region. Furthermore, the domain wall dynamics with a set of kink and antikink pair is developed. We will find that no annihilation of kinks occurs and the system keeps the number of walls invariant. Concluding remarks are given in Sec. IV.

II. OSCILLATORY PATTERN IN 1D SYSTEM AND ITS PHASE DYNAMICS

Let us consider the 1D aSH equation

$$\dot{w}(z,t) = [\epsilon - (\partial_z^2 + k_0^2)^2]w - |w|^2 w + \gamma w^* = -\frac{\delta \mathcal{H}}{\delta w^*} \tag{4}$$

with $\partial_z \equiv \partial/\partial z$, where

$$\mathcal{H} = \int dz\Bigg[-\epsilon|w|^2 - \frac{\gamma}{2}(w^2 + w^{*2}) + \frac{1}{2}(|w|^2)^2 + |(\partial_z^2 + k_0^2)w|^2 \Bigg] \tag{5}$$

denotes the Lyapunov functional of the system. Hereafter, without loss of generality, γ is chosen to be positive. By setting $w(z,t)=X(z,t)+iY(z,t)$, Eq. (4) is written as

$$\dot{X} = [\epsilon + \gamma - (\partial_z^2 + k_0^2)^2]X - (X^2 + Y^2)X, \tag{6a}$$

$$\dot{Y} = [\epsilon - \gamma - (\partial_z^2 + k_0^2)^2]Y - (X^2 + Y^2)Y. \tag{6b}$$

Equations (6) give the three types of stationary solutions X_0 and Y_0, i.e.,

(i) $X_0 = Y_0 = 0$,
(ii) $X_0 \neq 0$, $Y_0 = 0$,
(iii) $X_0 \neq 0$, $Y_0 \neq 0$,

which are, respectively, referred to as the trivial solution, the Néel type oscillatory solution and the Bloch type oscillatory solution. Of course, there exists another type of the solution $X_0=0$ and $Y_0 \neq 0$, which turns out to be unstable because the component X is more unstable than Y for $\gamma > 0$.

The linear stability of the trivial solution can be discussed with the linear growth rates for the wave number k mode around the solution

$$\lambda_k^X = \epsilon + \gamma - (k^2 - k_0^2)^2, \quad \lambda_k^Y = \epsilon - \gamma - (k^2 - k_0^2)^2. \tag{7}$$

The largest growth rates are $\epsilon+\gamma$ for X and $\epsilon-\gamma(<\epsilon+\gamma)$ for Y at $k=k_0$. Since the trivial solution is linearly stable for $\epsilon+\gamma<0$, we hereafter focus our attention on the case $\epsilon+\gamma>0$.

A. Néel type oscillatory pattern

Let us consider the dynamics of the Néel type oscillatory pattern, i.e., the solutions of Eqs. (6a) and (6b) with $Y=0$. We, therefore, try to solve the equations

$$\dot{X} = [\epsilon + \gamma - (\partial_z^2 + k_0^2)^2]X - X^3, \quad Y = 0. \tag{8}$$

This is identical to the conventional SH equation. If $X(z,t)$ is expanded as $X(z,t)=\sum_{n=-\infty}^{\infty}\rho_n(t)e^{ink_0 z}$ with $\rho_{-n}=\rho_n^*$, then the equations of motion for $\rho_n(t)$ are given by

$$\dot{\rho}_n = [\epsilon + \gamma - (n^2 - 1)^2 k_0^4]\rho_n - \sum_{k,l=-\infty}^{\infty} \rho_{n-k-l}\rho_k\rho_l. \tag{9}$$

As far as $0 < \epsilon+\gamma < k_0^4$, a solution $\rho_n=0$ for all n is linearly stable except for $n=\pm 1$, and the orders of ρ_n are estimated as $\rho_{\pm 1} \simeq \sqrt{(\epsilon+\gamma)/3}$, $\rho_{2n}=0$, and $\rho_{2n+1} \simeq O(\rho_1^{2n+1})$, respectively. If $\epsilon+\gamma$ is appropriately small, Eqs. (9) are reduced to the equation

$$\dot{\rho}_{\pm 1} = (\epsilon + \gamma)\rho_{\pm 1} - 3|\rho_1|^2\rho_{\pm 1} \tag{10}$$

by neglecting other terms than $\rho_{\pm 1}$ and the steady solution

$$X_0 = \rho_1 e^{ik_0 z} + \rho_{-1} e^{-ik_0 z} = \sqrt{4(\epsilon+\gamma)/3}\cos(k_0 z + \theta_0) \tag{11}$$

with a constant θ_0 is finally obtained. The steady solution can be obtained by setting $X=\rho\cos(k_0 z)$ and substituting it into Eq. (8), where higher harmonic terms proportional to $\cos(nk_0 z)$ and $\sin(nk_0 z)$ with $n>1$ are neglected.

In order to discuss the linear stability for the Néel type steady solution, we introduce disturbance variables u_x and u_y as

$$X(z,t) = X_0 + u_x, \quad Y(z,t) = Y_0 + u_y. \tag{12}$$

The linearization of Eq. (6b) around X_0 and $Y_0=0$ gives the perturbation equation for u_y,

$$\dot{u}_y = \Big[(\epsilon - \gamma) - \tfrac{4}{3}(\epsilon+\gamma)\cos^2(k_0 z) - (\partial_z^2 + k_0^2)^2\Big]u_y. \tag{13}$$

We can also obtain the perturbation equation for u_x. However, since u_x is linearly stable when we are concerned with

the instability of the Néel type solution, the equation of motion for u_x is not given here.

If one assumes the form $u_y(z,t)=\rho_c(t)\cos(k_0 z)+\rho_s(t)\sin(k_0 z)$ with z-independent ρ_c and ρ_s, Eq. (13) is alternatively written as

$$\dot{\rho}_c = -2\gamma\rho_c, \quad \dot{\rho}_s = \tfrac{2}{3}(\epsilon - 2\gamma)\rho_s, \tag{14}$$

where higher harmonic terms proportional to $\cos(3k_0 z)$ and $\sin(3k_0 z)$ are again neglected. Equation (14) and the stability of the trivial solution show that the Néel type oscillatory pattern is stable for $-\gamma<\epsilon<2\gamma$.

Let $\epsilon-2\gamma$ be negative. Then X grows exponentially at the first stage of the dynamics, but Y tends to vanish as time goes on. The eventual dynamics is therefore given by Eq. (8).

The spatially nonuniform modes around the wave number k_0 are excited in time. To take into account the temporal evolution, let X be divided into the amplitude variable ρ and the phase variable θ as

$$X(z,t) = \rho(z,t)\cos\,\theta(z,t), \tag{15}$$

where $|\partial_z\theta|$ is assumed to be close to k_0 as far as $\epsilon+\gamma$ is not so large. Substituting Eq. (15) into Eq. (8) with the assumption that the amplitude ρ approaches the constant $\rho_0=\sqrt{4(\epsilon+\gamma)/3}$ in a finite time leads to the phase equation

$$\dot{\theta} = \partial_z\{2[(\partial_z\theta)^2 - k_0^2]\partial_z\theta - \partial_z^2\partial_z\theta\} = -\frac{\delta\mathcal{H}_1\{\theta\}}{\delta\theta}, \tag{16}$$

where

$$\mathcal{H}_1\{\theta\} = \int dz\left\{\tfrac{1}{2}[(\partial_z\theta)^2 - k_0^2]^2 + \tfrac{1}{2}(\partial_z^2\theta)^2\right\}. \tag{17}$$

There exists a stable stationary solution $\theta(z)=k_0 z+\phi_0$ to Eq. (15) with any constant ϕ_0. We note that Eq. (16) coincides with the Kahn-Hilliard equation for the variable $u=\partial_z\theta$.

In the case of $\epsilon>2\gamma$, the Néel type oscillatory pattern becomes unstable and the Bloch type oscillatory pattern takes place as shown in the next section.

B. Bloch type oscillatory pattern

Next, we consider the dynamics for $\epsilon-2\gamma>0$. Under this condition, the imaginary part of the stationary solution $Y_0=0$ becomes linearly unstable. Thus one should set X and Y as

$$X = \rho_R\cos\,\theta_R, \quad Y = \rho_I\cos\,\theta_I \tag{18}$$

in order to develop the amplitude dynamics and the phase dynamics. Repeating the reduction procedure similar to that applied for the Néel oscillatory pattern, we obtain the amplitude equations

$$\dot{\rho}_R = (\epsilon+\gamma)\rho_R - g_1(\rho_R,\theta_R) - \tfrac{1}{2}(\rho_R^2+\rho_I^2)\rho_R - \tfrac{1}{4}\rho_R^3 - \tfrac{1}{4}\rho_I^2\rho_R\cos[2(\theta_I-\theta_R)], \tag{19a}$$

$$\dot{\rho}_I = (\epsilon-\gamma)\rho_I - g_1(\rho_I,\theta_I) - \tfrac{1}{2}(\rho_R^2+\rho_I^2)\rho_I - \tfrac{1}{4}\rho_I^3 - \tfrac{1}{4}\rho_R^2\rho_I\cos[2(\theta_R-\theta_I)] \tag{19b}$$

and the phase equations

$$-\rho_R\dot{\theta}_R = g_2(\rho_R,\theta_R) + \tfrac{1}{4}\rho_I^2\rho_R\sin[2(\theta_I-\theta_R)], \tag{20a}$$

$$-\rho_I\dot{\theta}_I = g_2(\rho_I,\theta_I) + \tfrac{1}{4}\rho_R^2\rho_I\sin[2(\theta_R-\theta_I)], \tag{20b}$$

where $g_1(\rho,\theta)$ and $g_2(\rho,\theta)$ are the functions of ρ, θ, and their derivatives. The derivation of the above equations and the explicit forms of g_1 and g_2 are provided in Appendix A. The stationary state with ρ_R^0, $\theta_R^0=k_0 z+\phi_R$, ρ_I^0, and $\theta_I^0=k_0 z+\phi_I$ with any constants ϕ_R and ϕ_I is thus evaluated by solving

$$0 = \rho_R^0\left[\epsilon+\gamma-\tfrac{1}{2}(\rho_R^{0^2}+\rho_I^{0^2}) - \tfrac{1}{4}\rho_R^{0^2} - \tfrac{1}{4}\rho_I^{0^2}\cos\{2(\theta_I^0-\theta_R^0)\}\right], \tag{21a}$$

$$0 = \sin[2(\theta_I^0-\theta_R^0)], \tag{21b}$$

$$0 = \rho_I^0\left[\epsilon-\gamma-\tfrac{1}{2}(\rho_R^{0^2}+\rho_I^{0^2}) - \tfrac{1}{4}\rho_I^{0^2} - \tfrac{1}{4}\rho_R^{0^2}\cos\{2(\theta_R^0-\theta_I^0)\}\right]. \tag{21c}$$

Equation (21b) leads to

$$2(\theta_I^0-\theta_R^0) = n\pi \tag{22}$$

for an arbitrary integer n. If n is an even number, then there are no solutions for ρ_R^0 and ρ_I^0 for $\gamma\neq 0$. On the other hand, if n is an odd number, then Eqs. (21a) and (21c) give the solution

$$\rho_R^0 = \sqrt{\epsilon+2\gamma}, \quad \rho_I^0 = \sqrt{\varepsilon-2\gamma}. \tag{23}$$

In studying the asymptotic process, we consider the case that ρ_R, ρ_I, θ_R, and θ_I vary slowly with respect to z, so both $g_1(\rho_R,\theta_R)$ and $g_1(\rho_I,\theta_I)$ can be neglected in Eqs. (19a) and (19b) in the lowest order with respect to the spatial variation. Since the characteristic times of ρ_R and ρ_I are much faster than those of θ_R and θ_I, ρ_R and ρ_I approach a quasi-steady-state which is characterized by $\dot{\rho}_R=\dot{\rho}_I=0$. This condition makes ρ_R and ρ_I be adiabatically integrated as

$$\rho_R^2 \simeq \rho_R^{0^2} - 2\left(\frac{\epsilon}{4}-\gamma\right)\cos^2(\theta_R-\theta_I), \tag{24a}$$

$$\rho_I^2 \simeq \rho_I^{0^2} - 2\left(\frac{\epsilon}{4}+\gamma\right)\cos^2(\theta_R-\theta_I), \tag{24b}$$

where we used $|\cos(\theta_R-\theta_I)|\ll 1$, noting that the phase difference $\theta_R-\theta_I$ is close to $n\pi/2$ from Eq. (22). By substituting Eqs. (24a) and (24b) into Eqs. (20a) and (20b), the phase equations are obtained in the forms

$$\dot{\theta}_R = -\frac{1}{4}\rho_I^{0^2}\sin[2(\theta_I-\theta_R)] - \frac{\delta\mathcal{H}_1\{\theta_R\}}{\delta\theta_R}, \tag{25a}$$

$$\dot{\theta}_I = -\frac{1}{4}\rho_R^{0^2}\sin[2(\theta_R-\theta_I)] - \frac{\delta\mathcal{H}_1\{\theta_I\}}{\delta\theta_I}, \tag{25b}$$

where $\mathcal{H}_1\{\theta\}$ is the same functional given by Eq. (17). In deriving Eqs. (25a) and (25b), these equations of motion are expanded with respect to $|\cos(\theta_R-\theta_I)|$ and the only lowest order is retained.

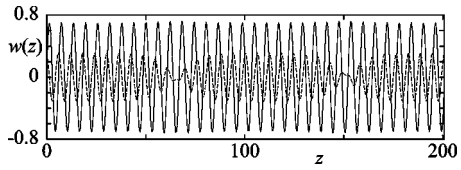

FIG. 1. Equation (4) is integrated by using the Euler method with the time step $\Delta t=1/2000$ and the space discretization width $\Delta z=\pi/8$ for the system size $L=512\Delta z$. The control parameters were set for $k_0=1$, $\epsilon=0.3$, and $\gamma=0.1$, and the initial state was generated by adding random numbers uniformly distributed in the range $[-0.01, 0.01]$ to the unstable uniform state $w_0=0$. Shown is a snapshot of $\mathrm{Re}[w(z,t)]$ (solid line) and $\mathrm{Im}[w(z,t)]$ (dashed line) at $t=2000$. One finds that there exists a domain with $\theta_I^0-\theta_R^0=\pi/2$ in the region of $70<x<150$ and a domain with $\theta_I^0-\theta_R^0=-\pi/2$ in the remaining region.

It is straightforward to prove that the stationary solutions Eq. (22) with odd n are linearly stable. One should note that although the above equations also have the synchronized stationary solution $\theta_R^0=\theta_I^0$ for $\gamma=0$, it is linearly unstable.

C. Domain wall dynamics in Bloch type oscillatory pattern

The fact that Eq. (4) has the two different stationary states $\theta_I^0-\theta_R^0=\pm\pi/2$ suggests that the two kinds of domains can be formed simultaneously in time. We numerically integrated Eq. (4) in terms of the explicit Euler scheme on a 1D lattice under a periodic boundary condition, where two control parameters were set as $\epsilon=0.3$ and $\gamma=0.1$ to satisfy the condition of forming the Bloch type oscillatory pattern. A snapshot is shown in Fig. 1. The figure indeed shows that the domain with $\theta_I^0-\theta_R^0=\pi/2$ coexists with that with $\theta_I^0-\theta_R^0=-\pi/2$, where a pair of domain walls are constructed to connect the domains.

In order to investigate the ordering process of the Bloch type oscillatory pattern, it is appropriate to introduce the difference variable $\mu(z,t)$ between two phases and the phase disturbance variable $\phi(z,t)$ through

$$\theta_R(z,t)=k_0z+\phi(z,t),\quad \theta_I(z,t)=k_0z+\phi(z,t)+\frac{\pi}{2}\mu(z,t), \tag{26}$$

where $\mu=+1$ and $\mu=-1$ correspond to $\theta_I^0-\theta_R^0=+\pi/2$ and $\theta_I^0-\theta_R^0=-\pi/2$, respectively. The equations of motion for μ and ϕ are obtained in the form $\dot{\phi}=f_1(\mu,\partial_z^2\phi,\ldots)$ and $\dot{\phi}+(\pi/2)\dot{\mu}=f_2(\mu,\partial_z^2\mu,\ldots)$ by substituting Eq. (26) into Eqs. (25a) and (25b). Assuming that ϕ and μ vary slowly with respect to z, one may approximately neglect higher-order differential terms than $\partial_z^2\phi$ and $\partial_z^2\mu$, and obtains a self-consistent equation for μ,

$$\dot{\mu}=\frac{\epsilon}{\pi}\sin(\pi\mu)+4k_0^2\partial_z^2\mu=-\frac{\delta\mathcal{H}_2\{\mu\}}{\delta\mu}, \tag{27}$$

where

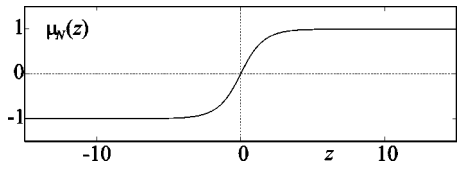

FIG. 2. The wall structure given in Eq. (30). The value of ξ evaluates the inverse of the domain width and is set to be one here.

$$\mathcal{H}_2\{\mu\}=\int dz\left[\frac{\epsilon}{\pi^2}\cos(\pi\mu)+2k_0^2(\partial_z\mu)^2\right]. \tag{28}$$

One can also obtain the equation of motion for ϕ of which the explicit form is not given here because the equation is not required in discussing the ordering process of the Bloch type oscillatory pattern.

Equation (27) has two stable uniform states $\mu=\pm1$ and one unstable uniform state $\mu=0$. One can analytically obtain a domain wall solution $\mu_N(z)$ by integrating the time-independent equation

$$\xi^2\sin(\pi\mu_N)+\partial_z^2(\pi\mu_N)=0,\quad \xi^2=\frac{\varepsilon}{4k_0^2} \tag{29}$$

under the boundary conditions $\mu_N=-1$ at $z=-\infty$ and $\mu_N=1$ at $z=\infty$. The above equation yields the solution

$$\mu_N(z)=1-\frac{4}{\pi}\arctan e^{-\xi z} \tag{30}$$

where the domain wall position is set at $z=0$. The width of the wall can be estimated as $1/\xi$. Equation (30) is known as the kink solution of the so-called sine-Gordon equation, whose explicit form with $\xi=1$ is drawn in Fig. 2.

Let us consider the time evolution in the case that a pair of a kink and an antikink exist at $z=z_1$ and $z=z_2$ on the condition of $z_1<z_2$, where the system locating two kinks at $z=z_1$ and $z=z_2$ is denoted as $\tilde{\mu}(z,t)$. We assume that $\tilde{\mu}(z,t)$ depends on time only through the drift motion of the two domain walls and that the pair annihilation process occurs when the distance of the walls becomes an order of $1/\xi$.

The drift motion of the domain wall existing at $z=z_i$ with $i=1$ or 2 is expressed by $\mu_N[z-z_i(t)]$, and therefore the time dependence of the system is approximately represented as a superposition of the two drifting domain walls

$$\tilde{\mu}(z,t)=\mu_N[z-z_1(t)]-\mu_N[z-z_2(t)]-1 \tag{31}$$

subject to the condition $z_2(t)-z_1(t)>1/\xi$. When $z_2(t)-z_1(t)$ becomes an order of $1/\xi$ in temporal evolution, annihilation of the two domain walls will occur.

As shown in Appendix B, substituting Eq. (31) into Eq. (27), which is multiplied by $\partial_z\tilde{\mu}(z,t)$, and then integrating it from $-\infty$ to $(z_1+z_2)/2$ gives the equation of motion for the domain wall position z_1 as

$$\dot{z}_1\simeq\frac{32\epsilon}{\pi^2\sigma}e^{-\xi(z_2-z_1)}, \tag{32}$$

where σ is the surface tension defined by

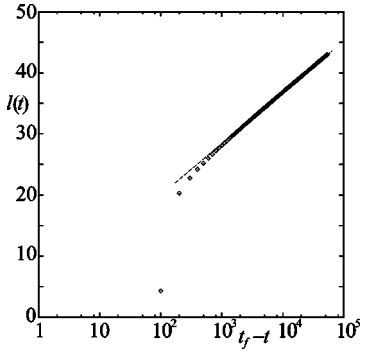

FIG. 3. Temporal evolution of the distance $\ell(t)$ between two domain walls. Theoretical form $\ell(t)=(2k_0/\sqrt{\epsilon})\ln[8\epsilon(t_f-t)]$ (dotted line), is compared to the simulation result (solid line) which is obtained by integrating Eq. (27) in terms of the Euler method with the time step $\Delta t=1/100$ and the space discretization width $\Delta z=1$ for the system size $L=128\Delta z$. The control parameters are set as $\epsilon=0.3$ and $k_0=1$.

$$\sigma \equiv \int_{-\infty}^{\infty} dz(\partial_z \mu_N)^2 = \frac{8\xi}{\pi^2}. \tag{33}$$

This method to obtain the dynamics for the position of the domain walls was originally developed by Nagai and Kawasaki [12] for the TDGL equation and is applied by Tutu and Fujisaka for the anisotropic TDGL equation [13]. Similarly, integrating the same equation from $(z_1+z_2)/2$ to ∞ gives the equation of motion for z_2 as

$$\dot{z}_2 \simeq -\frac{32\epsilon}{\pi^2\sigma} e^{-\xi(z_2-z_1)}. \tag{34}$$

Let $\ell \equiv z_2 - z_1$ denote the distance between the two domain wall positions. It immediately follows that

$$\dot{\ell} = -16k_0\sqrt{\epsilon}\exp\left(-\frac{\sqrt{\epsilon}}{2k_0}\ell\right), \tag{35}$$

where the explicit forms for ξ and σ provided by Eqs. (29) and (33) are substituted.

Equation (35) is straightforwardly integrated with the initial condition $\ell(t=0)=\ell_{st}$ to yield the form

$$\ell(t) = \frac{2k_0}{\sqrt{\epsilon}}\ln[8\epsilon(t_f - t)], \quad t_f \equiv \frac{1}{8\epsilon}\exp\left(\frac{\sqrt{\epsilon}}{2k_0}\ell_{st}\right), \tag{36}$$

where t_f, the time when the two domain walls annihilate, is uniquely determined via the initial distance ℓ_{st} between two domain walls. Equation (36) indicates that $\ell(t)$ decreases monotonously and the walls finally annihilate at time $t=t_f$. The theoretical result (36) is confirmed by the numerical simulation of Eq. (27) which is integrated with the same initial condition as in Eq. (36). The explicit time dependence of $\ell(t)$ evaluated by the numerical integration is shown in Fig. 3. One finds that $\ell(t)$ evolves logarithmically in time and the time evolution quantitatively agrees with the theoretical result (36).

The time dependence of $\ell(t)$ is furthermore confirmed by numerically integrating the original aSH equation (4). Figure 4 shows that the distance decreases logarithmically in time and the two domain walls annihilate at the time $t=t_f$. This characteristic agrees with the theoretical result (36). However, the rate of decrease is estimated to be 5.5, which is faster than the theoretically predicted one, $2k_0/\sqrt{\epsilon}\simeq 3.65$. The origin of this quantitative disagreement may be explained as follows. As is well known, the adiabatic elimination of amplitude is appropriate except for wall regions. We are now, on the other hand, discussing the dynamics of wall positions. So, in principle, the analysis in terms of the adiabatic elimination should lose its validity. Nevertheless, as shown above, the phase dynamics approach through the adiabatic elimination of amplitude seems to work qualitatively. Thus we suggest that if one attempts to compare the temporal evolutions of Eq. (36) with the numerical simulations, then one should take into account the fact that near wall amplitudes are less than (23). This fact may be phenomenologically taken into account by setting ϵ' which is smaller than ϵ. If ϵ in Eq. (36) is replaced by ϵ', the $\ell(t)$ becomes larger than that in Eq. (36), which tends to qualitatively agree with the observed result.

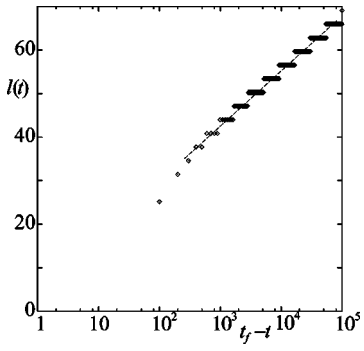

FIG. 4. Temporal evolution of the distance $\ell(t)$ between two domain walls which is obtained by integrating the original aSH equation (4) in terms of the Euler method with the time step $\Delta t=1/2000$ and the space discretization width $\Delta z=\pi/8$ for the system size $L=384\Delta z$. The control parameters are set as $k_0=1$, $\epsilon=0.3$, and $\gamma=0.1$. One finds that the asymptotic law $\ell(t)\simeq a\log(t_f-t)$ holds but the rate of decrease $a\simeq 5.5$ is larger than the theoretical one. Thus Eq. (27) turns out to qualitatively describe the domain dynamics of Eq. (4).

The temporal evolution starting from an initial state $w(z,0)\approx 0$ with parameter values for which the Bloch type oscillatory pattern stably exists is described as follows. In an early stage the amplitude exponentially grows towards the constant noted in Eq. (23). On the other hand, the phases evolve in time much slower than the amplitudes, with the result that the system tends to create many regions in each of which $\theta_I-\theta_R$ takes either $+\pi/2$ or $-\pi/2$. In this pattern, the wall positions separating $+\pi/2$ and $-\pi/2$ regions are randomly distributed. So the time evolution is asymptotically determined by Eq. (27) with randomly distributed $\mu=\pm 1$ regions and the domain walls connecting those domains.

A domain wall interacts with the neighboring walls in the form as in Eq. (35) and the distance between the walls decreases logarithmically as in Eq. (36), which yields the subsequent annihilations of domain walls and a decrease of the number of domains. Figure 5 shows the temporal evolution

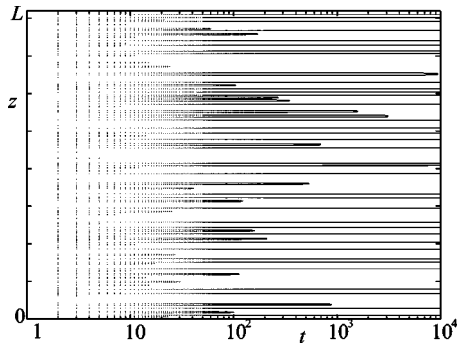

FIG. 5. Temporal evolution of the positions of domain walls $\overline{z}$, where $\overline{z}$ are evaluated as $\mu(\overline{z},t)=0$. Equation (27) is integrated for the system size $L=4096\Delta z$. Other parameters are set to be the same as in Fig. 3. For details, see the text.

of domain wall positions $\overline{z}$ which are determined via the condition $\mu(\overline{z},t)=0$. One finds that the characteristic domain size grows in time due to the annihilations of domain walls.

Let $\langle \ell(t) \rangle$ denote the average domain size at time t evaluated by the system size L divided by the number of domain walls $n(t)$, i.e.,

$$\langle \ell(t) \rangle = \frac{L}{n(t)}. \tag{37}$$

Since the lifetime τ of a domain with length ℓ is proportional to $e^{\sqrt{\epsilon}\ell/2k_0}$, $n(t)$ is estimated by solving the equation

$$\dot{n} \simeq -\frac{1}{\tau} \propto -e^{-(\sqrt{\epsilon}/2k_0)\langle \ell(t) \rangle}. \tag{38}$$

Equations (37) and (38) yield the equation for $\langle \ell(t) \rangle$, which reveals that the average domain size grows logarithmically in time, i.e., $\langle \ell(t) \rangle \propto \log t$ in a late stage. Figure 6 confirms numerically that $\langle \ell(t) \rangle$ increases logarithmically as time goes on.

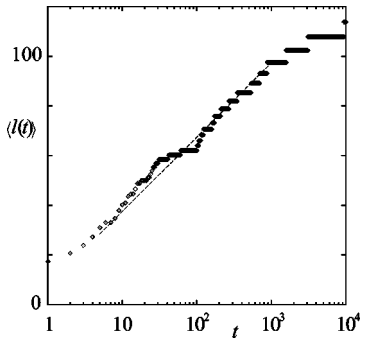

FIG. 6. Temporal evolution of the average domain size $\langle \ell(t) \rangle$. The simulation result and the logarithmic line are denoted by the diamond symbol and the dashed line, respectively. One finds that the average domain size increases logarithmically as time goes on.

III. DOMAIN WALLS IN THE 1D SYSTEM

A. Uniform steady states and their stabilities

There exist several nontrivial uniform states in Eq. (4) depending on parameter values. We first find spatially uniform states w_0's and then discuss their stabilities.

w_0's are determined by solving

$$0 = (\epsilon - k_0^4)w_0 - |w_0|^2 w_0 + \gamma w_0^*. \tag{39}$$

There exist five uniform states

$$w_0 = \begin{cases} 0, & \\ \pm\sqrt{\epsilon+\gamma-k_0^4} & \text{for } \epsilon+\gamma-k_0^4 > 0, \\ \pm i\sqrt{\epsilon-\gamma-k_0^4} & \text{for } \epsilon-\gamma-k_0^4 > 0. \end{cases} \tag{40}$$

To examine the stability of their uniform states, we introduce a disturbance variable $\psi(z,t)$ by

$$w(z,t) = w_0 + \psi(z,t). \tag{41}$$

The linearized equation of ψ is written as

$$\dot{\psi} = [\epsilon - (\partial_z^2 + k_0^2)^2]\psi - 2|w_0|^2\psi - w_0^2\psi^* + \gamma\psi^*. \tag{42}$$

By setting $\psi = \psi_R + i\psi_I$, Eq. (42) is re-expressed as

$$\dot{\psi}_R = [\epsilon + \gamma - 2|w_0|^2 - w_0^2 - (\partial_z^2 + k_0^2)^2]\psi_R, \tag{43a}$$

$$\dot{\psi}_I = [\epsilon - \gamma - 2|w_0|^2 + w_0^2 - (\partial_z^2 + k_0^2)^2]\psi_I. \tag{43b}$$

Equations (43) immediately reveal that the uniform state w_0 is stable for perturbations with any wave number k if the conditions

$$\epsilon + \gamma - 2|w_0|^2 - w_0^2 < 0, \tag{44a}$$

$$\epsilon - \gamma - 2|w_0|^2 + w_0^2 < 0 \tag{44b}$$

are both satisfied. The stability of individual uniform states in Eq. (40) is examined as follows.

(i) $w_0=0$: This trivial solution is unstable because $\epsilon+\gamma$ is always larger than 0.

(ii) $w_0 = \pm i\sqrt{\epsilon-\gamma-k_0^4}$: Substituting these solutions into Eq. (44a) leads to

$$2\gamma + k_0^4 < 0, \tag{45}$$

which is never satisfied because of $\gamma > 0$ and so the two uniform states are both unstable.

(iii) $w_0 = \pm\sqrt{\epsilon+\gamma-k_0^4}$: Substituting these solutions into Eqs. (44a) and (44b) and leads leads to

$$\gamma > -\epsilon + (3/2)k_0^4, \quad \gamma > (1/2)k_0^4, \tag{46}$$

respectively. If ϵ and γ are implemented to satisfy these inequalities, where $\epsilon+\gamma-k_0^4>0$ is automatically satisfied, then the uniform states are linearly stable.

B. Néel type wall

The fact that the two uniform states $w_0 = \pm\sqrt{\epsilon+\gamma-k_0^4}$ $(\equiv \pm W_0)$ are stable under condition (46) suggests that Eq. (4)

has several domain wall solutions. Indeed, as will be shown soon, two kinds of domain walls are found; these are discriminated by whether or not the imaginary part vanishes. The former and the latter are referred to as the Néel type domain wall and the Bloch type domain wall, respectively.

Let us first discuss the Néel type (i.e., real) solution $w_N(z)$ of Eq. (4). The parameters ϵ and γ are hereafter implemented to satisfy the inequalities (46). The solution is obtained by solving the time-independent SH equation

$$(\partial_z^2 + k_0^2)^2 w_N = (\epsilon + \gamma) w_N - w_N^3 \quad (w_N = w_N^*) \tag{47}$$

under the boundary conditions $w_N = -W_0$ at $z = -\infty$ and $w_N = W_0$ at $z = \infty$. One is not capable of solving Eq. (47) strictly, so that we attempt to obtain an asymptotic form

$$w_N(z) \simeq \pm W_0 + \zeta(z) \quad \text{for } z \to \pm\infty, \tag{48}$$

where $\zeta(z)$ is an odd function of z and denotes the deviation from the uniform state W_0. Without loss of generality, the domain wall position is set at $z=0$. By substituting Eq. (48) into Eq. (47), the equation for $\zeta(z)$ is obtained in the form

$$(\partial_z^2 + k_0^2)^2 \zeta = \Gamma \zeta, \tag{49}$$

where $\Gamma \equiv \epsilon + \gamma - 3W_0^2 (= k_0^4 - 2W_0^2)$ takes a negative value because of the condition (44a). Equation (49) is solved by setting

$$\zeta(z) = \frac{A}{2} e^{\lambda z + i\phi} + \text{c.c.}, \tag{50}$$

where A and ϕ are positive constants and λ is a complex number satisfying the equation $(\lambda^2 + k_0^2)^2 = \Gamma$. As a consequence, one finds the solution

$$w_N(z) = \pm W_0 \pm A e^{-|z|/z_0} \cos(Q|z| - \phi) \tag{51}$$

for $z \to \pm\infty$, where A and ϕ are constants which are not determined in the above linearized theory. z_0 and Q measure the domain width and the wave front oscillation, respectively, and take the forms

$$z_0 = \sqrt{\frac{2}{\sqrt{2} W_0 - k_0^2}}, \quad Q = \sqrt{\frac{1}{2}(\sqrt{2} W_0 + k_0^2)}. \tag{52}$$

C. Bloch type wall

Let us next consider the Bloch type (i.e., complex) solution $w_B(z)$ of Eq. (4), which is obtained by solving the time-independent aSH equation

$$(\partial_z^2 + k_0^2)^2 w_B = \epsilon w_B - |w_B|^2 w_B + \gamma w_B^* \tag{53}$$

under the same boundary condition as for the Néel type wall. It is assumed that $w_B(z)$ can be set in a similar way to Eq. (48),

$$w_B(z) \simeq \pm W_0 + \zeta(z) \quad \text{for } z \to \pm\infty, \tag{54}$$

where $\zeta(z)$ is now a complex function whose real part is odd and imaginary part is even with respect to z. The domain wall position is set to be $z=0$. The substitution of Eq. (54) into Eq. (53) gives the equation for $\zeta(z)$ of the form

$$(\partial_z^2 + k_0^2)^2 \zeta = \epsilon \zeta - W_0^2 (2\zeta + \zeta^*) + \gamma \zeta^*. \tag{55}$$

By setting $\zeta = \zeta_R + iq\zeta_I$, where q takes the value 1 or -1 corresponding to the sign of the imaginary part of w_B at $z=0$, Eq. (55) is re-expressed as

$$(\partial_z^2 + k_0^2)^2 \zeta_R = \Gamma_R \zeta_R, \quad (\partial_z^2 + k_0^2)^2 \zeta_I = \Gamma_I \zeta_I, \tag{56}$$

where both $\Gamma_R \equiv \varepsilon + \gamma - 3W_0^2 (= k_0^4 - 2W_0^2)$ and $\Gamma_I \equiv \varepsilon - \gamma - W_0^2 (= k_0^4 - 2\gamma)$ take negative values because of the conditions (44a) and (44b). Equation (56) is solved in the same way as that of the Néel type wall, and one obtains the asymptotic form

$$\begin{aligned} w_B(z) = {} & \pm W_0 \pm A_R e^{-|z|/z_R} \cos(Q_R|z| - \phi_R) \\ & + iqA_I e^{-|z|/z_I} \cos(Q_I|z| - \phi_I) \end{aligned} \tag{57}$$

for $z \to \pm\infty$, where A_R, A_I, ϕ_R, and ϕ_I are constants. Here, z_R, z_I, Q_R, and Q_I are given by

$$\begin{aligned} & 1/z_R = \sqrt{\tfrac{1}{2}(\sqrt{2} W_0 - k_0^2)}, \quad Q_R = \sqrt{\tfrac{1}{2}(\sqrt{2} W_0 + k_0^2)}, \\ & 1/z_I = \sqrt{\tfrac{1}{2}(\sqrt{2\gamma} - k_0^2)}, \quad Q_I = \sqrt{\tfrac{1}{2}(\sqrt{2\gamma} + k_0^2)}. \end{aligned} \tag{58}$$

D. Numerical forms of the Néel wall and the Bloch wall

It is quite difficult, as mentioned earlier, to find exact solutions of Eqs. (47) and (53) analytically. We therefore try to obtain the explicit forms of Néel type and Bloch type walls by solving the equations numerically. Instead of solving Eqs. (47) and (53) and directly, Eq. (4) is integrated numerically because the forms satisfying the equations (47) or (53) are obtained via integration for a sufficiently long time to lead to steady states.

Equation (4) is integrated with the Euler scheme. The control parameter ϵ is fixed to $3/2$, and γ is set to be 0.47, where the uniform states w_0 are linearly unstable, and 0.51, 0.55, 0.58, and 0.59, where w_0 are stable due to condition (46).

Both the oscillatory pattern solution discussed in Sec. II and the wall solutions are stable for the above parameter value and therefore they coexist. Thus in order to find the wall solution (except $\gamma = 0.47$ case), numerical integration is carried out by imposing the artificial initial condition $X(z,0) \approx -W_0$ for $z < z_0$, $X(z,0) \approx W_0$ for $z >= z_0$ and $Y(z,0) \approx 0$. The Neumann boundary condition is adopted due to the initial condition.

The results are depicted in Fig. 7. Figure 7(a) shows that the oscillatory pattern is observed instead of the domain wall due to the uniform states w_0 being unstable. Figures 7(b)–7(d) show that the Bloch type walls $w_B(z)$ are stable for $0.5 < \gamma < 0.59$ where $\mathrm{Im}[w(z)] \neq 0$ in the vicinity of the domain wall position. Figure 7(e) shows that the Néel type wall emerges in place of the Bloch type wall for $\gamma \geqslant 0.59$, where $\mathrm{Im}[w(z)] = 0$ for any z.

E. Domain wall dynamics

The time evolution in the case that a pair of kink and an antikink exists at $z = z_1$ and $z = z_2$, respectively, is investigated

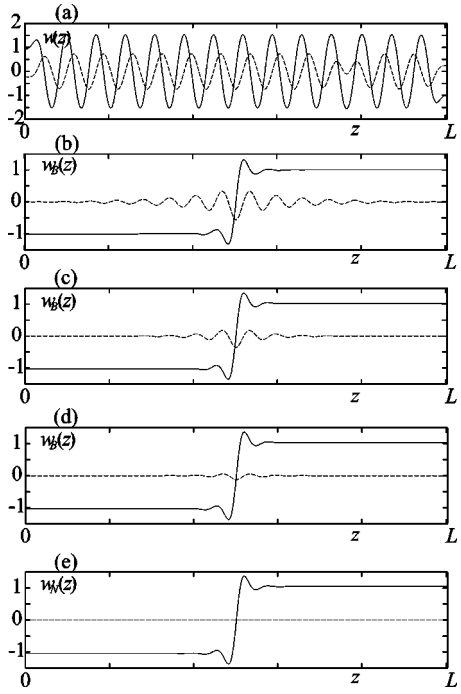

FIG. 7. Snapshots of the Néel type wall and several Bloch type walls. The forms of these walls are obtained by numerically integrating Eq. (4) with $\Delta t=1/6000$ and $\Delta z=\pi/16$ for the system size $L=512\Delta z$. The control parameter k_0 and ϵ are fixed to be 1 and 3/2, respectively, and γ is set to be (a) 0.47, (b) 0.51, (c) 0.55, (d) 0.58, and (e) 0.59. For details, see the text.

in this section. The time dependence of the system is approximately represented as a superposition of the two domain walls located at $z_1(t)$ and $z_2(t)$ at time t, i.e.,

$$\tilde{w}(z,t) = w_K[z - z_1(t)] - w_K[z - z_2(t)] - W_0, \tag{59}$$

where $\tilde{w}$ satisfies Eq. (4). Here w_K denotes either w_N or w_B according to the dynamics of the Néel type wall or the Bloch type wall.

As shown in Appendix C, substituting Eq. (59) into Eq. (4) and applying the method by Nagai and Kawasaki, one finds that the equation of motion of the distance $\ell(t)=z_2(t)-z_1(t)$ between the two domain walls obeys

$$\dot{\ell} = \frac{1}{\sigma}\left[\Phi\left(\frac{z_1+z_2}{2}\right) - \Phi(\infty)\right], \tag{60}$$

where $\Phi(z)$ is a function of $\tilde{w}$ and its derivatives defined by

$$\Phi(z) = (\epsilon - k_0^4)|\tilde{w}|^2 + \frac{\gamma}{2}[(\tilde{w})^2 + (\tilde{w}^*)^2] - \frac{1}{2}(|\tilde{w}|^2)^2 - [2k_0^2|\partial_z\tilde{w}|^2 + \partial_z^2(|\partial_z\tilde{w}|^2) - 3|\partial_z^2\tilde{w}|^2] \tag{61}$$

and σ is the surface tension

$$\sigma \equiv \int_{-\infty}^{\infty} |\partial_z w_K(z)|^2\, dz. \tag{62}$$

We first derive the equation of motion for $\ell(t)$ when the Néel type wall stably exists. Here $\tilde{w}$ results in the real function, i.e., $\tilde{w}=\tilde{w}^*$, in Eq. (61). By substituting the asymptotic

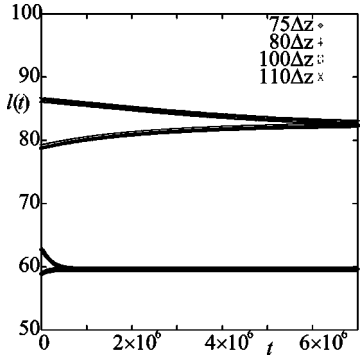

FIG. 8. Time dependence of the distance between two domain walls initially separated by several lengths. The initial distance of two walls is set as $\ell_{st}=n\Delta z$ with $n=75$, 80, 100, and 110. Equation (4) is integrated with $\Delta t=1/2000$ and $\Delta z=\pi/4$ for the system size $L=256\Delta z$. The control parameters are set as $k_0=1/4$, $\epsilon=1.5k_0^4$, and $\gamma=0.6k_0^4$. For details, see the text.

Néel type wall solution (51) into Eq. (60), one obtains

$$\sigma\dot{\ell} = 4A^2\sqrt{2W_0^2(2W_0^2 - k_0^4)}e^{-\ell/z_0}\sin(Q\ell - 2\phi - 2\theta), \tag{63}$$

where Q is same as in Eq. (52), and θ is a constant phase defined by

$$\sin 2\theta = \frac{\sqrt{2W_0^2 - k_0^4}}{\sqrt{2W_0^2}}. \tag{64}$$

Equation (63) reveals that the distance $\ell(t)$ between the two domain walls, which is initially set to be a value ℓ_{st}, begins to shrink if $\sin(Q\ell_{st}-2\phi-2\theta)<0$ and spreads out if $\sin(Q\ell_{st}-2\phi-2\theta)>0$. Therefore, the distance in the limit $t\to\infty$ approaches a definite length ℓ_n, which is determined by $Q\ell_n-2\phi-2\theta=(2n+1)\pi$ with an integer n. The selected ℓ_n is the nearest to ℓ_{st}.

The time dependence of $\ell(t)$ is evaluated numerically in order to examine the above theoretical result. Figure 8 shows the temporal evolution for four initial distances $\ell_{st}=75\Delta z$, $80\Delta z$, $100\Delta z$, and $110\Delta z$ with $\Delta z=\pi/4$. For the runs with the initial distances $75\Delta z$ and $80\Delta z$, they approach the length $\ell_n\simeq 59$. For the runs with $100\Delta z$ and $110\Delta z$, they eventually approach the length $\ell_{n+1}\simeq 82$. The above results are consistent with the relation $Q(\ell_{n+1}-\ell_n)=2\pi$ since $Q\simeq 0.28$ for the above parameter values. One further notices that the two domain walls starting at the distances $\ell_{st}=100\Delta z$ and $110\Delta z$ move much slower than the wall movement starting at $\ell_{st}=75\Delta z$ and $80\Delta z$ as a result of the relation $\dot{\ell}\propto e^{-\ell/z_0}$. The result is confirmed via the numerical simulation for another parameter value, $\epsilon=1.5k_0^4$ and $\gamma=0.8k_0^4$ with $k_0=1/4$, and we obtained the result consistent with the theoretical one.

In the above discussion, we evaluated the value of $\Phi((z_1+z_2)/2)$ in terms of a simple superposition of the two perturbatively obtained solutions (51) which are derived from the linear stability analysis of the homogeneous solution W_0. So we have revealed that the time evolution of the

distance $\ell(t)$ between the two domain walls is determined with the linear stability analysis around the middle of the two domain walls.

Next we turn to the derivation of the equation of motion for $\ell(t)$ when the Bloch type wall stably exists. By substituting the asymptotic Bloch type wall solution (57) into Eq. (60), one obtains

$$\sigma\dot{\ell} = 4A_R^2\sqrt{2W_0^2(2W_0^2-k_0^4)}e^{-\ell/z_R}\sin(Q_R\ell - 2\phi_R - 2\theta_R) - 4q_1q_2A_I^2\sqrt{2\gamma(2\gamma-k_0^4)}e^{-\ell/z_I}\sin(Q_I\ell - 2\phi_I - 2\theta_I), \tag{65}$$

where z_R, z_I, Q_R, and Q_I are given in Eq. (58). q_1 and q_2 represent the directions of the imaginary part of the Bloch type wall at $z=z_1$ and $z=z_2$, respectively. θ_R is identical to that given in Eq. (64), while θ_I is defined by

$$\sin 2\theta_I = \frac{\sqrt{2\gamma-k_0^4}}{\sqrt{2\gamma}}. \tag{66}$$

The condition (46) yields the inequality $z_I > z_R$ and so that the first term of Eq. (65) is neglected, leading to

$$\sigma\dot{\ell} \simeq -4q_1q_2A_I^2\sqrt{2\gamma(2\gamma-k_0^4)}e^{-\ell/z_I}\sin(Q_I\ell - 2\phi_I - 2\theta_I). \tag{67}$$

Equation (67) reveals that the direction of motion of $\ell(t)$ starting at ℓ_{st} is determined not only by the sign of the quantity $\sin(Q_I\ell_{st}-2\phi_I-2\theta_I)$ but also by the sign of q_1q_2, which takes +1 when the imaginary parts of the two domain walls exist on the opposite side of direction and takes −1 when on the same direction. Nevertheless, the distance again approaches a definite value with a constant ℓ_n, similarly to the Néel type wall case.

Let us consider the 1D anisotropic TDGL equation,

$$\dot{\psi} = \psi - |\psi|^2\psi + \gamma\psi^* + \partial_z^2\psi, \tag{68}$$

where ψ is the complex spin order parameter and γ is the strength of anisotropy. It is well known that the above equation has the Bloch wall solution for $0<\gamma<1/3$. As shown in Refs. [13,14], the distance $\ell(t)$ of a pair of the Bloch walls obeys the equation of motion

$$\dot{\ell} = -q_1q_2\frac{8\sqrt{2\gamma}(1-3\gamma)}{1-\gamma/3}e^{-\sqrt{2\gamma}\ell}, \tag{69}$$

which does not contain the term $\sin(Q_I\ell-2\phi_I-2\theta_I)$ existing in Eq. (67). Equation (69) shows that the distance $\ell(t)$ shrinks and eventually disappears for $q_1q_2>0$, or spreads out infinitely for $q_1q_2<0$ in the limit $t\to\infty$, which is different from the time evolution in the Bloch type wall in the present case.

IV. CONCLUDING REMARKS

In this paper, we have investigated two types of asymptotic dynamics in an anisotropic, complex Swift-Hohenberg equation (4), especially focusing on the interaction between the neighboring domain walls.

The first type of dynamics is the asymptotic pattern formation process in the case that spatially oscillatory patterns are formed. The oscillatory patterns are distinguished according to whether or not the imaginary part of the field $w(z,t)$ vanishes. It was shown that the imaginary part vanishes ($Y_0=0$) for $-\gamma<\epsilon<2\gamma$, which is referred to as the Néel type oscillatory pattern by analogy with the time-dependent Ginzburg-Landau equation, and that the dynamics becomes identical to the conventional, real Swift-Hohenberg equation.

On the other hand, the stationary solution $Y_0=0$ becomes unstable provided that the condition $\epsilon>2\gamma$ is satisfied, so that both the real and imaginary parts form a spatially oscillatory pattern, which is referred to as the Bloch type oscillatory pattern. In this case, there exist two stable states in which the phase difference of the oscillation between the real and imaginary part takes either the value $\pi/2$ or $-\pi/2$. These two states form a kind of domain structure and the coexistence of the distinct domains constructs the domain walls in temporal evolution.

We derived the equation of motion for the phase difference and discussed the time evolution of two domain walls with the use of the method originally developed by Nagai and Kawasaki. It was revealed that the distance between two domain walls decreases logarithmically and the walls finally annihilate at a characteristic time uniquely determined via the initial distance between the walls. Qualitative agreement between the theoretical analysis and the numerical experiment was obtained by comparing several numerical simulations.

The second type of dynamics is the asymptotic pattern formation process in the case where the nontrivial uniform states stably exist. The two uniform states $w_0=\pm\sqrt{\epsilon+\gamma-k_0^4}$ are linearly stable when ϵ and γ are implemented to satisfy the inequalities (46). It was found that there exist two distinguishable domain walls according to whether or not the imaginary parts of the walls vanish. One of them is the Néel type domain wall for the vanishing imaginary part and the other the Bloch type domain wall for non-vanishing imaginary part in the vicinity of the wall. The asymptotic forms of two kinds of domain walls were analytically derived and were compared to the numerically obtained results.

The equations of motion of the distances between the two Néel type domain walls and the two Bloch type domain walls were then derived. We found that the distance between two domain walls approaches a definite length even in the limit $t\to\infty$, although the distance in the early stage begins to shrink or spread out according to the initial state. This characteristic holds irrespective of whether the domain wall is the Néel type or the Bloch type.

ACKNOWLEDGMENTS

The authors thank H. Tutu for valuable comments. This study was partially supported by Grant-in-Aid for Scientific Research (C) of the Ministry of Education, Culture, Sports, Science, and Technology, and the 21st Century COE Program "Center Of Excellence for Research and Education on Complex Functional Mechanical Systems" at Kyoto University.

APPENDIX A: PHASE DYNAMICS FOR THE aSH EQUATION

In this Appendix, we will derive the equations of motion (19) for the amplitudes ρ_R and ρ_I and the equations of motion (20) for the phases θ_R and θ_I from the aSH equation (6). Before developing the reduction procedure, we first introduce the notation

$$(\partial_z^2 + k_0^2)\rho e^{i\theta} = [f_1(\rho,\theta) + i f_2(\rho,\theta)]e^{i\theta}, \tag{A1}$$

where $f_1(\rho,\theta)$ and $f_2(\rho,\theta)$ are expressed as

$$f_1(\rho,\theta) = \partial_z^2\rho + [k_0^2 - (\partial_z\theta)^2]\rho,$$

$$f_2(\rho,\theta) = 2(\partial_z\rho)(\partial_z\theta) + \rho\partial_z^2\theta. \tag{A2}$$

It should be noted that $f_1(\rho_0, k_0 z+\phi_0) = f_2(\rho_0, k_0 z+\phi_0) = 0$ holds for any constants ρ_0 and ϕ_0. Furthermore we define $g_1(\rho,\theta)$ and $g_2(\rho,\theta)$ by

$$(\partial_z^2 + k_0^2)^2\rho e^{i\theta} = [g_1(\rho,\theta) + i g_2(\rho,\theta)]e^{i\theta}, \tag{A3}$$

where the quantities $g_1(\rho,\theta)$ and $g_2(\rho,\theta)$ are expanded as

$$g_1(\rho,\theta) = \partial_z^2 f_1 + [k_0^2 - (\partial_z\theta)^2]f_1 - 2(\partial_z\theta)(\partial_z f_2) - f_2\partial_z^2\theta,$$

$$g_2(\rho,\theta) = \partial_z^2 f_2 + [k_0^2 - (\partial_z\theta)^2]f_2 + 2(\partial_z\theta)(\partial_z f_1) + f_1\partial_z^2\theta. \tag{A4}$$

The equality $g_1(\rho_0, k_0 z+\phi_0) = g_2(\rho_0, k_0 z+\phi_0) = 0$ again holds for any constants ρ_0 and ϕ_0.

Substituting $X = \rho_R \cos\theta_R$ and $Y = \rho_I \cos\theta_I$ into Eq. (6a) and using the relation $(\partial_z^2 + k_0^2)^2(\rho_R \cos\theta_R) = g_1^R \cos\theta_R - g_2^R \sin\theta_R$ provided by Eq. (A3), one obtains

$$\begin{aligned}
&\dot\rho_R \cos\theta_R - \rho_R\dot\theta_R \sin\theta_R \\
&\quad = (\epsilon+\gamma)\rho_R\cos\theta_R - (g_1^R\cos\theta_R - g_2^R\sin\theta_R) \\
&\qquad - \tfrac{1}{4}\rho_R^3(\cos 3\theta_R + \cos\theta_R) - \tfrac{1}{4}\rho_R\rho_I^2[\cos(2\theta_I+\theta_R) \\
&\qquad + \cos\theta_R\cos\{2(\theta_I-\theta_R)\} - \sin\theta_R\sin\{2(\theta_I-\theta_R)\}] \\
&\qquad - \tfrac{1}{2}(\rho_R^2+\rho_I^2)\rho_R\cos\theta_R.
\end{aligned} \tag{A5}$$

The comparison of the left-hand side with the right-hand side for terms proportional to $\cos\theta_R$ and $\sin\theta_R$ leads to Eqs. (19a) and (20a), respectively, where higher harmonics $\cos 3\theta_R$ and $\cos(2\theta_I+\theta_R)$ are neglected.

Equations (19b) and (20b) are obtained in a similar way by substituting $X = \rho_R\cos\theta_R$ and $Y = \rho_I\cos\theta_I$ into Eq. (6b).

APPENDIX B: EQUATION OF MOTION FOR THE DOMAIN WALL POSITION IN THE BLOCH TYPE OSCILLATORY PATTERN

Let us derive the equation of motion (32) for the domain wall located at the position $z = z_1$. The time evolution in the existing two domain walls denoted as Eq. (31) is described by Eq. (27). Multiplication of each side of Eq. (27) by $\partial_z\tilde\mu$ leads to

$$\begin{aligned}
&-\dot z_1[(\partial_z\mu_{N1})^2 - (\partial_z\mu_{N1})(\partial_z\mu_{N2})] + \dot z_2[(\partial_z\mu_{N1})(\partial_z\mu_{N2}) \\
&\qquad - (\partial_z\mu_{N2})^2] = \partial_z\Phi(z),
\end{aligned}$$

$$\Phi(z) = -\frac{\epsilon}{\pi^2}\cos\pi\tilde\mu + 2k_0^2(\partial_z\tilde\mu)^2, \tag{B1}$$

where the notation $\mu_{Ni} = \mu_N[z - z_i(t)]$ has been used for simplicity. If the distance $|z_2 - z_1|$ between the two walls is much larger than the domain width $1/\xi$ which was introduced in Eq. (29), then the integration of Eq. (B1) from $-\infty$ to $(z_1+z_2)/2$ leads to

$$-\sigma\dot z_1 = \Phi\left(\frac{z_1+z_2}{2}\right) - \Phi(-\infty), \tag{B2}$$

where σ is the surface tension given in Eq. (33). We have used the relation

$$\int_{-\infty}^{\infty}(\partial_z\mu_{Ni})(\partial_z\mu_{Nj})dz = \sigma\delta_{ij}, \tag{B3}$$

which holds because the differentiation of Eq. (30),

$$\partial_z\mu_{Ni}(z) = \frac{2\xi}{\pi}\frac{1}{\cosh[\xi(z-z_i)]} \tag{B4}$$

is a sharp function located at the vicinity of $z = z_i$.

The right-hand side of Eq. (B2) is evaluated as follows. The asymptotic form of Eq. (30),

$$\mu_N(\pm z) \simeq \pm 1 \mp \frac{4}{\pi}e^{-\xi z} \quad \text{for } z \gg 1/\xi \tag{B5}$$

gives

$$\tilde\mu\left(\frac{z_1+z_2}{2}\right) = \mu_N\left(\frac{\ell}{2}\right) - \mu_N\left(-\frac{\ell}{2}\right) - 1 = 1 - \frac{8}{\pi}e^{-\xi\ell/2} \tag{B6}$$

with $\ell = z_2 - z_1$. On the other hand, Eq. (B4) yields

$$\partial_z\tilde\mu\left(\frac{z_1+z_2}{2}\right) = \partial_z\mu_N\left(\frac{\ell}{2}\right) - \partial_z\mu_N\left(-\frac{\ell}{2}\right) = 0. \tag{B7}$$

The substitution of these results and the obvious relations $\tilde\mu(-\infty) = -1$ and $\partial_z\tilde\mu(-\infty) = 0$ into Eq. (B2) leads to Eq. (32).

APPENDIX C: EQUATION OF MOTION FOR POSITIONS OF THE NÉEL TYPE WALL AND THE BLOCH TYPE WALL

Let w_K be either the Néel type wall solution (51) or the Bloch type wall solution (57). Consider the integral

$$\begin{aligned}
&\int_{-\infty}^{(z_1+z_2)/2}[(\partial_z\tilde w)\dot{\tilde w}^* + (\partial_z\tilde w^*)\dot{\tilde w}^*]dz \\
&\quad = \int_{-\infty}^{(z_1+z_2)/2}((\partial_z\tilde w)\{[\epsilon - (\partial_z^2+k_0^2)^2]\tilde w^* \\
&\qquad + \gamma\tilde w - |\tilde w|^2\tilde w^*\} + (\partial_z\tilde w^*) \\
&\qquad \times\{[\epsilon - (\partial_z^2+k_0^2)^2]\tilde w + \gamma\tilde w^* - |\tilde w|^2\tilde w\})dz,
\end{aligned} \tag{C1}$$

where $\tilde w(z,t)$ is denoted by Eq. (59). If the distance $|z_2 - z_1|$ between the two walls is much larger than the domain wall

width described either by Eq. (52) in the case of the Néel type wall or by Eq. (58) in the case of the Bloch type wall, then the left-hand side of Eq. (C1) is evaluated as

$$\begin{aligned}\mathrm{LHS} &= \int_{-\infty}^{(z_1+z_2)/2} (\partial_z w_{K1} - \partial_z w_{K2})(-\dot{z}_1 \partial_z w_{K1}^* \\ &\quad + \dot{z}_2 \partial_z w_{K2}^*) dz + \text{c.c.} \\ &\simeq -2\int_{-\infty}^{(z_1+z_2)/2} (\dot{z}_1 |\partial_z w_{K1}|^2 + \dot{z}_2 |\partial_z w_{K2}|^2) dz \\ &\simeq -2\sigma \dot{z}_1, \end{aligned} \tag{C2}$$

where $w_{Ki} \equiv w_K[z - z_i(t)]$ and σ is the surface tension denoted by Eq. (62). The right-hand side of Eq. (C1) is, on the other hand, expressed in the form

$$\mathrm{RHS} = \int_{-\infty}^{(z_1+z_2)/2} \partial_z \Phi(z) dz = \Phi\left(\frac{z_1+z_2}{2}\right) - \Phi(-\infty), \tag{C3}$$

where $\Phi(z)$ is defined by Eq. (61). Equation (C2) with (C3) gives the equation of motion for the left wall position $z_1(t)$.

Then the integration from $(z_1+z_2)/2$ to ∞ leads to the equation for the right domain wall position $z_2(t)$,

$$-2\sigma \dot{z}_2 = \Phi(\infty) - \Phi\left(\frac{z_1+z_2}{2}\right). \tag{C4}$$

Equations (C2)–(C4) immediately yield Eq. (60) by making use of the relation $\Phi(-\infty) = \Phi(\infty)$.

In the Néel type wall, Eq. (59) is represented as

$$\begin{aligned}\tilde{w}(z,t) &= W_0 + Ae^{-(z-z_1)/z_0} \cos[Q(z-z_1) - \phi] \\ &\quad + Ae^{(z-z_2)/z_0} \cos[Q(z-z_2) + \phi], \end{aligned} \tag{C5}$$

where A and ϕ are constants, and the nth derivative of Eq. (C5) is obtained by

$$\begin{aligned}\partial_z^n \tilde{w}(z,t) &= (-\alpha)^n A e^{-(z-z_1)/z_0} \cos[Q(z-z_1) - \phi - n\theta] \\ &\quad + \alpha^n A e^{(z-z_2)/z_0} \cos[Q(z-z_2) + \phi + n\theta] \end{aligned} \tag{C6}$$

where θ is a constant phase defined by Eq. (64) and $\alpha = \sqrt{\sqrt{2}W_0}$. Substituting the above expressions of $\tilde{w}((z_1+z_2)/2, t)$ and $\partial_z^n \tilde{w}((z_1+z_2)/2, t)$ into Eq. (61) and retaining terms with $e^{-\ell/2z_0}$ and $e^{-\ell/z_0}$ where $\ell \equiv z_2 - z_1$ by noting that ℓ is large yields Eq. (63). A similar derivation leads to the asymptotic dynamics of Bloch type walls.

[1] J. D. Gunton, M. S. Miguel, and P. S. Sahni, *Phase Transitions and Critical Phenomena* (Academic, New York, 1983).
[2] H. Furukawa, Adv. Phys. **34**, 703 (1985).
[3] A. J. Bray, Adv. Phys. **43**, 357 (1994).
[4] P. Manneville, *Dissipative Structures and Weak Turbulence* (Academic, Boston, 1990).
[5] M. C. Cross and P. C. Hohenberg, Rev. Mod. Phys. **65**, 851 (1993).
[6] P. G. de Gennes, *Physics of Liquid Crystals* (Clarendon, Oxford, 1982).
[7] S. Chandrasekhar, *Liquid Crystals* (Cambridge University Press, Cambridge, 1977).
[8] E. Meron, Phys. Rep. **218**, 1 (1992).
[9] K. Kawasaki and T. Ohta, Physica A **116**, 573 (1982).
[10] T. Nagai and K. Kawasaki, Physica A **120**, 587 (1983).
[11] K. Kawasaki and T. Nagai, Physica A **121**, 175 (1983).
[12] T. Nagai and K. Kawasaki, Physica A **134**, 483 (1986).
[13] H. Tutu and H. Fujisaka, Phys. Rev. B **50**, 9274 (1994).
[14] H. Tutu, Phys. Rev. E **67**, 036112 (2003).
[15] M. Mino, S. Miura, K. Dohi, and H. Yamazaki, J. Magn. Magn. Mater. **226–230**, 1530 (2001).
[16] S. Miura, M. Mino, and H. Yamazaki, J. Phys. Soc. Jpn. **70**, 2821 (2001).
[17] J. Swift and P. C. Hohenberg, Phys. Rev. A **15**, 319 (1977).
[18] K. Ouchi and H. Fujisaka, Phys. Rev. E **54**, 3895 (1996).
[19] M. Le Berre *et al.*, Phys. Rev. E **66**, 026203 (2002).